Acta Materialia 179 (2019) 201–214

Contents lists available at ScienceDirect

Acta Materialia

journal homepage: www.elsevier.com/locate/actamat

Full length article

Physical metallurgy-guided machine learning and artificial intelligent design of ultrahigh-strength stainless steel

Chunguang Shen [a], Chenchong Wang [a, **], Xiaolu Wei [a], Yong Li [a], Sybrand van der Zwaag [b], Wei Xu [a, *]

[a] State Key Laboratory of Rolling and Automation, Northeastern University, Shenyang, Liaoning, 110819, China
[b] Novel Aerospace Materials Group, Faculty of Aerospace Engineering, Delft University of Technology, 2629 HS, Delft, the Netherlands

ARTICLE INFO

Article history:
Received 15 June 2019
Received in revised form
5 August 2019
Accepted 18 August 2019
Available online 20 August 2019

Keywords:
Alloy design
Machine learning
Physical metallurgy
Small sample problem
Stainless steel

ABSTRACT

With the development of the materials genome philosophy and data mining methodologies, machine learning (ML) has been widely applied for discovering new materials in various systems including high-end steels with improved performance. Although recently, some attempts have been made to incorporate physical features in the ML process, its effects have not been demonstrated and systematically analysed nor experimentally validated with prototype alloys. To address this issue, a physical metallurgy (PM) -guided ML model was developed, wherein intermediate parameters were generated based on original inputs and PM principles, e.g., equilibrium volume fraction (V_f) and driving force (D_f) for precipitation, and these were added to the original dataset vectors as extra dimensions to participate in and guide the ML process. As a result, the ML process becomes more robust when dealing with small datasets by improving the data quality and enriching data information. Therefore, a new material design method is proposed combining PM-guided ML regression, ML classifier and a genetic algorithm (GA). The model was successfully applied to the design of advanced ultrahigh-strength stainless steels using only a small database extracted from the literature. The proposed prototype alloy with a leaner chemistry but better mechanical properties has been produced experimentally and an excellent agreement was obtained for the predicted optimal parameter settings and the final properties. In addition, the present work also clearly demonstrated that implementation of PM parameters can improve the design accuracy and efficiency by eliminating intermediate solutions not obeying PM principles in the ML process. Furthermore, various important factors influencing the generalizability of the ML model are discussed in detail.

1. Introduction

Given its very high strength, good toughness and excellent corrosion resistance, ultrahigh-strength (UHS) stainless steels have been used as a high-performance structural material for the nuclear, gear, bearing, aerospace and other high-end industries [1–3]. To obtain superior mechanical properties, many systematic experimental studies have been performed to optimize their composition and heat treatment parameters [4–6]. Although many UHS stainless steels with excellent properties were successfully developed via systematic experiments, the experimental trial and error approach is considered inefficient, limiting its capacity to explore unknown domains [7,8].

Considering advances in the understanding of ferrous metallurgy, PM has become increasingly important for guiding new alloy design by means of physical modelling and property predictions, especially for UHS stainless steels [9–12]. Various models have been built to describe (i) microstructure evolution, i.e., the correlations between the composition/process and microstructure, and (ii) the microstructure/property relationship of such steels. Regarding the first topic, composition/processing relations were used as input to predict various microstructure characteristics using corresponding PM models (e.g., evolution of the lath martensite grain size with variation of carbon content and tempering time [13], evolution of the dislocation density during ageing [14] and

* Corresponding author. State key laboratory of rolling and automation, Northeastern University, Shenyang, Liaoning, 110819, China.
** Corresponding author.
E-mail addresses: shenchunguang@stumail.neu.edu.cn (C. Shen), wangchenchong@ral.neu.edu.cn (C. Wang), weixiaolu@stumail.neu.edu.cn (X. Wei), neuliyong@stumail.neu.edu.cn (Y. Li), S.vanderZwaag@tudelft.nl (S. van der Zwaag), xuwei@ral.neu.edu.cn (W. Xu).

https://doi.org/10.1016/j.actamat.2019.08.033
1359-6454/

evolution of element solubility with temperature variation [15]). Regarding the second topic, quantitative microstructural characteristics obtained from experimental observation, calculated results by PM models or arbitrary assumptions were used as inputs to predict the mechanical response, in particular the yield strength, the ultimate tensile strength and the toughness. For example, physical models have been built to describe various strengthening mechanisms, such as classical precipitation strengthening by Orowan dislocation looping [16] and Friedel's shear cutting [17], solid-solution strengthening by Fleischer's model [18], dislocation strengthening by the Kocks-Mecking model [19] and grain boundary strengthening by the Hall-Petch model [20,21]. Therefore, the yield strength can be well predicted considering the overall contribution of the aforementioned mechanisms and hence be used to guide the design and optimization of alloy composition and heat treatment conditions [9,12,22]. In Olson's work [12], comprehensive experimental techniques, e.g., local-electrode atom-probe (LEAP) tomography and electron back-scattered diffraction (EBSD), were employed to obtain detailed microstructural inputs for PM models of microstructure/property correlations. In addition to experimental inputs, a number of physical parameters in PM models were extracted from the literature, which is a time consuming and risky approach considering the differences in alloy systems and experimental conditions. Moreover, as most UHSS alloys are strengthened by multiple types of precipitates, e.g., M_2C, M_3C and Cu (bcc), the strengthening contribution of each type of precipitate is calculated separately and their contributions are summed. The linear superposition law greatly increases the complexity, and inheritance of inevitable modelling errors in each of the strengthening contributions represents a great difficulty in obtaining a reliable prediction of the final overall properties. In the work of Nava [9], the yield strength was calculated by superimposing the contributions of different strengthening mechanisms and multiple precipitates. In that publication, the PM model for each maraging steel group had dedicated parameter value sets, indicating the instability of the solution and its low generalization level. Furthermore, although the reverted/retained austenite is a key factor influencing the mechanical properties of maraging steels [23], their effects were ignored, yet good agreement could be obtained [24]. Apparently, the ML adjusted fit parameter sets for strengthening mechanisms taken into account, can 'correct' for strengthening factors not considered. An alternative alloy design approach does not use actual steel property datasets but to stay closer to thermodynamic predictions and incorporate them in the design algorithms. In Xu's research, UHS stainless steel and creep-resistant steel were designed by combining PM models, thermodynamics and a GA [25–29]. GA methods help to search for the optimal solution in an extremely large solution space combining composition and key heat treatment parameters, but the lack of actual microstructure information still limits the accuracy of PM models and inhibits the design efficiency. In summary, although advanced characterization techniques, comprehensive literature data search/extraction and standardized thermodynamic models have been employed to obtain various microstructure information and physical parameters, prediction errors were inevitably introduced to the PM modelling process owing to experimental uncertainties and system complexity, especially for multiple precipitation strengthening systems. Moreover, the implementation of key microstructure features, e.g., retained austenite, plays a key role in the actual mechanical properties yet represent great difficulties in the modelling. Furthermore, when microstructure information acts as a bridge connecting two links, the errors generated in the 'composition/microstructure link would be accumulated and amplified in the next 'microstructure/properties' link, which would eventually impede the accurate prediction of mechanical properties.

In addition to the experimental trial and error approach and PM model approach, artificial intelligence methods, especially ML, for property prediction and material design have attracted a lot of attention. Already in the 1950s, researchers started to explore methods, such as the perceptron [30], to make machines acquire knowledge using various symbolic methods. Later, methods based on the connection principle, e.g., artificial neural networks (ANNs), were widely studied. More recently, more comprehensive methods, such as support vector machines (SVMs), based on statistical learning theory were developed. Various material properties were successfully predicted by the abovementioned ML models [31–36]. For example, Sha et al. successfully established an ANN model connecting the composition, processing parameters, working conditions and mechanical properties of maraging steels using a database of 2959 samples. Good accuracy in terms of R^2, i.e., above 90% and 85% for the training and testing sets, respectively, was achieved [37]. Based on a much smaller database, the corrosion rate of 3C steel in different environments was precisely predicted using an SVM trained on only 46 samples, and the deviation between the predicted and experimental values was less than 0.5 $\mu A\,cm^{-2}$ [38]. The capability of ML prediction strongly depends on the size and quality of the databases as well as the range and distribution of the input parameters. Under ideal conditions SVM can be successfully applied with only 46 samples and reach a high prediction accuracy, while an ANN would require much more data. In general, ML systems are rarely viewed in the context of small data, where an insufficient data size for the training model compromises the learning success. The bottleneck of the database size especially limits applications in steel development, in which the construction of a database via experiments is time consuming and costly. Moreover, it is very important to notice that, although various ML approaches could establish direct purely statistics-based correlations between composition/processing inputs and output target properties without considering any microstructural characteristics, the lack of underlying microstructure information, i.e., the essential link between composition/processing and mechanical properties, and ignoring metallurgical interactions and principles, represent great risks in model predictions, increase the dependence on the quality of the database and impede further analysis or interpretation with physical mechanisms. Recently, SISSO (Sure Independence Screening and Sparsifying Operator) approach has been developed [39], which can reduce immense features spaces to low-dimensional spaces based on compressed-sensing, to predict target property of material using various physical descriptors. However, meanwhile it was state that [39], although physical parameters can participate in model training, a simple, analytical descriptor-property function may not even exist, and it is mainly applied to simple-structure material, rather than metallic material with complex microstructure. In addition, Shin et al. trained ML models by integrating microstructure-related synthetic/scientific features to predict creep behaviour of high-temperature alloys and demonstrated that it could be regarded as an intermediate tool to facilitate new alloy design insights and approaches to guide prototype alloy selection and experimental validation [40], although it neither clearly demonstrated positive effects of incorporating scientific features on improving the accuracy, nor validated the approach by newly designed prototype alloy. Although ML essentially correlates input parameters with output target properties for the composition range covered in the data set and has no design function itself, under certain conditions it can be applied to discover new systems in combination with a proper search algorithm [41–46]. For example, an ANN model coupling composition/processing variable with various mechanical properties was established and combined with a GA to design new micro-alloyed

pipeline steel and cold rolled IF steels [41,43]. Large amounts of design results are usually obtained in a ML design process, so how to quickly identify quality of design results is also a key issue. In the research of Lu et al. [47], the performance of hybrid organic-inorganic perovskites (HOIPs) was calculated by combining a ML model with the density functional theory. The bandgaps for the structures of 5158 HOIPs in the search space were predicted using the ML model, and all HOIP candidates were screened step-by-step using the DFT theory and taking into account various features. Although ultimately six lead-free orthorhombic HOIPs with proper bandgaps were successfully identified, this screening method based on input from separate additional calculations might be inefficient for large-scale optimization studies.

In the design of new materials based on ML methods, the design process can be roughly divided into four steps: 1) database construction from literature data or own experimental observations, 2) ML model development linking input parameters and output properties based on the database, 3) search and first evaluation of new input dataset targeting superior output in the vast candidate space and 4) identification of newly designed candidate solutions for experimental validation. For step 1, the size and quality of the database are essential, and inputs/outputs must be defined appropriately. For step 2, a reliable ML model for the database at hand is required to maximize the learning capacity. In addition to the purely statistical ML approaches presented in the literature, the guidance of embedded PM principles may significantly increase the prediction accuracy, which will be discussed in this paper. For step 3, a proper search algorithm must be employed to explore the vast candidate space and find good candidate solutions. In the last step, the searching methodology generally yields a larger number of good solutions and a proper intelligent screening methodology may be needed for selection or identification of the most promising solution worth a costly experimental validation. Following this procedure, in the present work, a ML approach combining supported vector machine and guidance from PM principles (SVM-PM model) was developed to predict the correlation of input (composition/process) and output (hardness) for UHS stainless steels while considering the key microstructure information as a guideline to increase learning performance. To this aim the predictions of the SVM-PM model are probed in a GA to evaluate the vast solution space and explore the optimal composition and ageing conditions. Finally, a new support vector classifier (SVC) was employed to screen potential candidates from the previous step and select a limited number of solutions for experimental validation. A newly designed alloy was fabricated and processed as designed, and superior properties were obtained. As will be shown the PM variables played a considerable role in the ML model, and its effects in guiding the learning capacity are discussed. In particular, important factors of the generalizability of the SVM model, i.e., the PM variables, partition of the training and testing sets, kernel function, features and precipitate species in the dataset, discussed in detail.

2. Hardness prediction by PM-guided ML

2.1. Dataset and parameters

In the present work, compositions and hardness data from various UHS stainless steels reported in the literature were collected and grouped according to their principal strengthening precipitates, including the R-phase (102 samples) [48], Cu clusters (124 samples) [49–54], and Ni_3Ti (116 samples) [55–57]. These datasets are provided in the supplementary information. All steels belong to the family of martensitic stainless steels and were produced via (complete) homogenisation-quenching-tempering routes. The R-phase dataset was used to train the SVM-PM model and design new alloys of UHS stainless steel with a high hardness due to strengthening by the R-phase. The other datasets were used to study the generalizability of the model. The steel composition and conditions during thermal processing are the most straightforward parameters to determine the microstructure, e.g., the content and morphology of the martensite matrix, retained austenite and precipitates, and hence the mechanical properties. With the main strengthening precipitate being pre-defined, the ageing temperature and ageing time were selected as the main thermal processing parameters. Unlike conventional ML database constructions is which take only the original inputs, e.g., composition and process parameters, and build a direct correlation with target output properties, as discussed earlier, the microstructure characteristics are the essential link bridging the original inputs and target output properties; thus, these characteristics must be considered in an appropriate way. Nevertheless, the microstructure information is very difficult, if not possible, to extract in a standardized manner from the literature. Moreover, the contribution of precipitation strengthening mainly depends on both the V_f and the (average) size of the precipitates. The size of the precipitates has a close relationship with nucleation kinetics, which is mainly controlled by the thermodynamic D_f. Therefore, intermediate PM parameters representing microstructure features, i.e., V_f and D_f, were also introduced as model inputs. V_f and D_f were calculated by Thermo-Calc® software using the TCFE9 database. The experimental hardness was set as the output target, and important statistics of the model features are listed in Table 1. R-phase could not precipitate in some samples due to the relatively low ageing temperature, e.g. 300 °C. Therefore, minimum of V_f and D_f was zero and negative respectively. Because all samples used in the datasets underwent the same smelting process, solution treatment and quenching, these features are assumed to have had no effect on the hardness and were ignored in training the SVM-PM model.

The quality of the input dataset which may significantly but in an unknown or unrecorded manner depend on the experimental conditions or even human factors, is critical for the reliability of the prediction. In order to minimize those deviations, in this work, the mechanical property focuses on Rockwell hardness, which is not

Table 1
Input and output ranges used in the SVM (i.e. steels containing R-phase precipitates) modelling.

	Inputs and output	Minimum	Maximum	Mean	Standard deviation
Inputs	Carbon (wt.%)	0.002	0.09	0.03	0.03
	Chromium (wt.%)	11.90	15.00	12.58	1.20
	Nickel (wt.%)	1.50	6.00	4.39	1.03
	Cobalt (wt.%)	11.40	20.00	13.03	2.47
	Molybdenum (wt.%)	2	5.30	4.37	0.91
	Titanium (wt.%)	0	0.20	0.12	0.10
	Ageing temp (°C)	300	600	498.77	60.27
	Ageing time(hour)	3.16	4.00	3.65	0.41
	V_f (%)	0	8.46	5.68	2.60
	D_f (J/mol)	−262	1072	492	324
Output	Hardness (HRC)	26.4	51.0	43.5	5.5

Table 2
Hardness measurement in the present work and corresponding literature data [48]. Compositions are in weight percentages. Temperature and time are in Celsius and hour, respectively. Hardness is in Rockwell.

Fe	C	Cr	Ni	Co	Mo	T_{Age}	t_{age}	Reported hardness	Measured hardness
Balance	0.002	15.00	2.50	15.00	5.00	500	3.16	48.9	47.8(±0.2)
						525	3.16	49.3	48.1(±0.1)
						550	3.16	49.8	49.7(±0.5)

very sensitive to test conditions. Moreover, the dataset of R-phase is extracted from an identical research group, which greatly reduces risks of arbitrary fluctuations. Nevertheless, to ascertain data reliability and transferability one alloy from the literature was fabricated and heat treated with identical conditions as mentioned in the literature and a very good agreement has been observed as shown in Table 2. The reproducibility of the literature data indicates the reliability of the dataset. Two PM parameters introduced, i.e., V_f and D_f, are calculated by Thermo-Calc® with the most recent database TCFE9, of which the calculation reliability is widely accepted. In addition, calculations on all literature systems involved show that the R-phase is the primary strengthening precipitate even with all possible phases activated in the Thermo-Calc® calculation.

2.2. Modelling process

A conventional normalization method was applied to eliminate dimensional differences between the parameter ranges and to enhance the accuracy of the SVM-PM model. The inputs and outputs were normalized by the z-score method [58], given by Eq. (1):

$$z = \frac{x - \mu}{\sigma} \tag{1}$$

where z denotes the normalized data, x is the original data from the datasets, and μ and σ represent the mean and standard deviation of the original data, respectively.

The kernel function, which embeds samples into a high-dimensional feature space, is very important for the generalization ability of SVM models. In the present work, a radial basis function (RBF) kernel, which is suitable for nonlinear problems, was selected [59]. The generalization ability of SVM with RBF is controlled by two critical parameters, C and γ [60]. C is the penalty parameter in the objective function of SVM, and it was set as a constant greater than zero. Overestimation of C would lead to overfitting, while underestimating of C value would result in underfitting. Parameter γ determines the distribution of data mapped to a new feature space and the number of support vectors. Different algorithms can be used to optimize C and γ combinations, such as grid search and heuristic algorithms. In this work, a GA was applied to search for optimal parameter combinations. The search process for optimal parameters was operated with 500 generations, and the search ranges for parameters C and γ were 0–500 and 0–100, respectively.

The dataset of the R-phase contained 102 samples in total; 80 samples were randomly selected as the training set, which was used to optimize parameters in SVM-PM models with RBF, and the other 22 samples were used as the testing set for the generalization ability of the SVM-PM models. Given the very limited amount of data in present work (only 102 samples), the performance of trained model greatly varies with different partitions of training and testing sets. Moreover, a random partition of dataset is prone to unbalanced data distribution, which will lead to unfair evaluation of the model performance. Therefore, to better evaluate the generalization ability of the SVM-PM model, the 'multiple hold-out method' was employed for the partition of training and testing sets, in which the dataset was randomly divided into training and testing sets by 500 times to build 500 different SVM-PM models, and the mean and maximum of evaluation function of all 500 SVM-PM models were taken as the evaluation indices. The effects of different partitions will be addressed in the discussion. Then, the squared correlation coefficient (R^2) and mean absolute error (MAE) were adopted to evaluate the generalization ability of the SVM-PM models. The calculation methods are given by Eqs. (2) and (3):

$$R^2 = \frac{\left(n\sum_{i=1}^{n} f(x_i)y_i - \sum_{i=1}^{n} f(x_i)\sum_{i=1}^{n} y_i\right)^2}{\left(n\sum_{i=1}^{n} f(x_i)^2 - \left(\sum_{i=1}^{n} f(x_i)\right)^2\right)\left(n\sum_{i=1}^{n} y_i^2 - \left(\sum_{i=1}^{n} y_i\right)^2\right)} \tag{2}$$

$$MAE = \frac{1}{n}\sum_{i=1}^{n} |f(x_i) - y_i| \tag{3}$$

where n is the number of samples and $f(x_i)$ and y_i represent the predicted and experimental values of the i_{th} sample, respectively.

2.3. Hardness prediction

Because 500 different partitions of the training and testing sets were applied, each sample could participate into training and testing sets multiple times; hence, multiple predictions could be obtained for each sample. Therefore, the mean and maximum values of R^2 and MAE of each data point were calculated to evaluate the generalization ability of the SVM-PM model. The prediction results are shown in Fig. 1. Mean results and optimal results for both the training and testing sets are shown in Fig. 1a–b and Fig. 1c–d, respectively. In Fig. 1a–d, most points in both the training and testing sets lie on or very close to the straight line with a slope of 1, which strongly indicates that most of the predicted values are in good agreement with experimental values. This result implies that the SVM-PM model has excellent generalization ability and high prediction accuracy. Considering that the SVM-PM model will be further used to design new UHS stainless steels, the performance of the testing set is more important than that of the training set. As shown in Fig. 1b and d, the mean and maximum values of R^2 for the testing set were 92.9% (±3.9%) and 98.25%, respectively, and the mean and minimum values of MAE were 1.15 HRC (±1.1 HRC) and 0.75 HRC (±0.42 HRC). Regarding the mean prediction results of the 500 SVM-PM models in Fig. 1b and 70 of the 102 samples had absolute errors between the experimental and predicted values within 1.0 HRC, and the maximum absolute error was 4.5 HRC. Regarding the optimal prediction results of the 500 SVM-PM models in Fig. 1d and 16 of the 22 samples had absolute errors less than 1 HRC, and the maximum absolute error was only 1.9 HRC. In summary, both the mean and maximum values exhibited an extremely small deviations between the experimental hardness and the predicted hardness, which indicates that the parameters as found for the final SVM-PM model are applicable to the entire dataset.

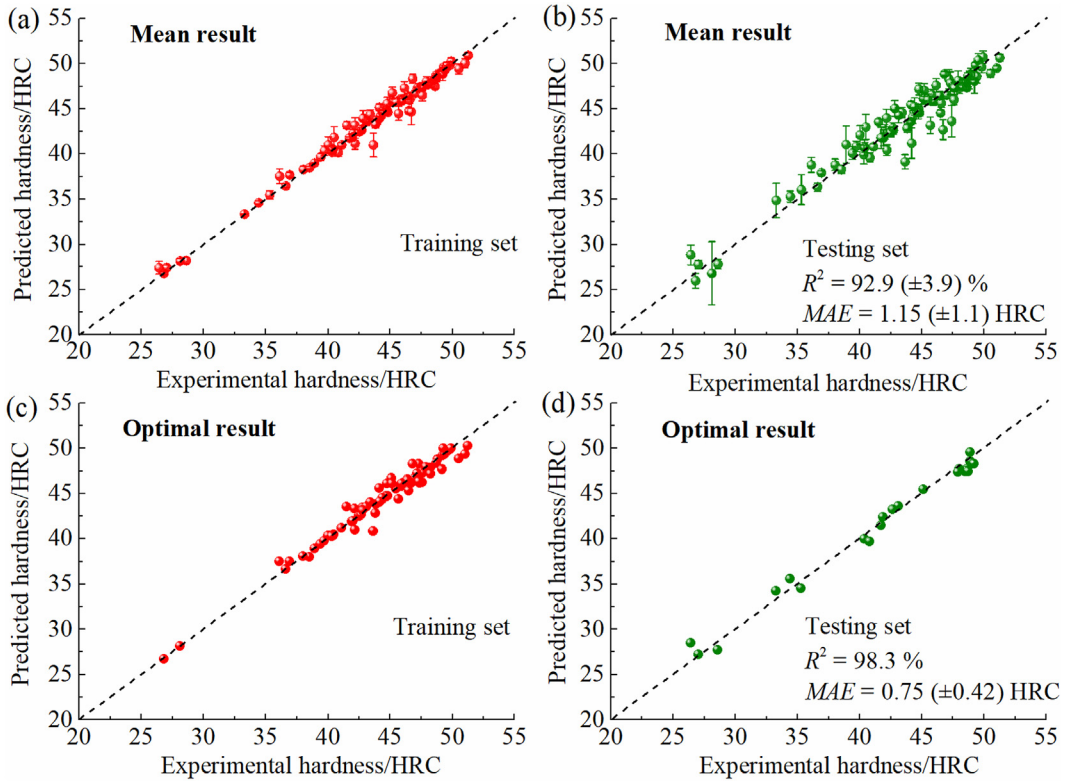

Fig. 1. Experimental values vs. values predicted by the SVM-PM model for 500 different partitions of the training and testing sets: (a) training set of mean result; (b) testing set of mean result; (c) training set of optimal result; (d) testing set of optimal result.

3. Alloy design combining the SVM-PM model and a GA

3.1. Design process

Improved alloy composition and ageing conditions of UHS stainless steel strengthened by the R-phase precipitates were designed within the original parameter range in the dataset by combining the SVM-PM model and a GA for optimization (SVM-PM&GA). The output prediction of the SVM-PM model was used as an objective function of the GA, and it established the relationship between the composition/process parameters and the hardness. The GA was applied to search for the optimal alloy composition and ageing conditions to obtain a high hardness. The optimization was performed over many generations until the output did not change for 10 consecutive iterations, likely indicating convergence. A schematic of the design process is shown in Fig. 2.

As stated earlier, 500 random partitions of the training and testing sets were used to construct the SVM-PM model. Then, the hardness of the samples in the testing set was predicted by 500 different models. In this design exercise, the confidence of designed results by GA directly depended on the generalization ability of the objective function from the SVM-PM model, and therefore models of higher R^2 were preferred. However, to maintain the model diversity associated with different partitioning, a substantial number of models were required. To make the balance of high generalization ability and good diversity, a criterion of R^2 >95%, i.e., 155 best models out of 500 possible models, was enforced in the design process. For each of the 155 selected SVM-PM models, the GA was applied to find a new solution (composition, ageing temperature and ageing time) with the maximal hardness. Therefore, 155 new alloys can be designed following this approach. However, not all of the newly designed alloy possessed hardness values beyond the original maximum value in the dataset (51 HRC). In this case, 39 of the 155 design results were removed as they yielded lower maximal values.

3.2. Model validation by SVC model

With 155 SVM-PM models selected on the basis of the criterion of R^2 >95%, the 155 design GA exercise yielded 155 designed solutions, among which 116 solutions were predicted to outperform the existing alloys. However, in order to determine a limited number of prototype alloys for experimental validation in the present work, a classifier was applied to further refine the solution for experimental validation. The classifier was trained based on the complete experimental dataset to filter solutions with hardness above 49 HRC, and subsequently applied to 116 optimal solutions so as to obtain solutions in the category of 'high hardness', which gave the highest likelihood to experimentally outperform existing alloys.

The SVC model was applied to evaluate the 116 optimal solutions by classifying them into 'high hardness" and 'low hardness', as shown in "Model validation by calculations" in Fig. 2. The SVC model determined the category of the optimal solution by identifying the combination of the composition and ageing conditions. Samples in the dataset with hardness values less than 49 HRC were given the label −1, representing 'low hardness'. In contrast, samples with hardness values greater than 49 HRC were given the label 1, representing 'high hardness'. Furthermore, the original dataset was used as a training set to train the SVC classifier to enable the classifier to learn the characteristic features of different categories. The

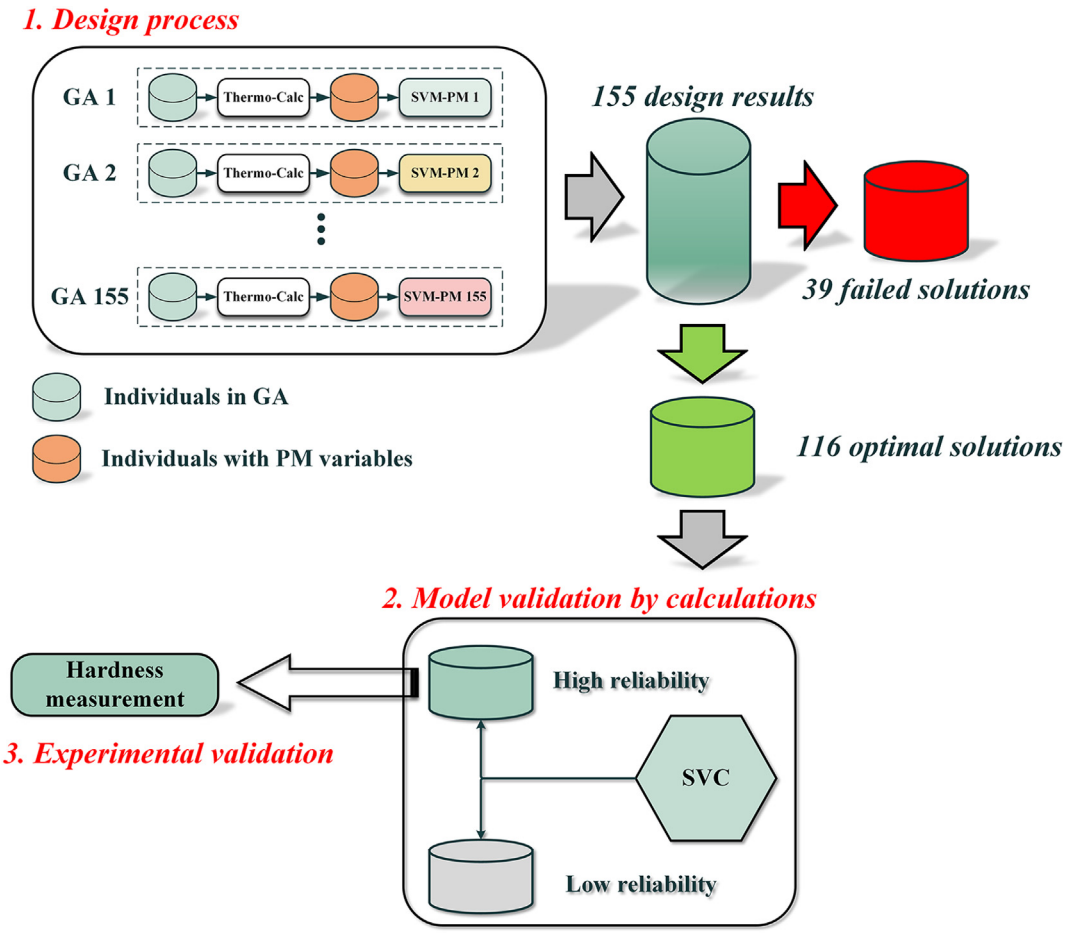

Fig. 2. Schematic diagram of the design method and model validation.

z-score method was applied to eliminate dimensional differences, and the grid search method was used to optimize parameters of the SVC classifier. Finally, the SVC model was successfully constructed, and the classification accuracy was 96%. To classify design results, the 116 optimal solutions were used as the testing set and divided into 'high hardness' and 'low hardness' by the SVC model. As a result, only 11 optimal solutions were classified as 'high hardness', and the other design results were defined as "low hardness".

In order to show the spatial distribution of the 116 newly designed optimal solutions, all solutions are positioned according to their PM parameters, i.e., V_f and D_f, as shown in Fig. 3. It can be observed that, although optimal solutions are distributed in a large space, there is still a clear tendency of clustering in the region of high V_f and D_f, which makes perfect sense from a metallurgical point of view. Moreover, all 11 solutions validated by classifier are highlighted in the plot, all located in the upright region of the possible solution, with a limited dispersion. However, more detailed examination of those 11 solutions reveals that, the dispersion originates more from the ageing temperature, while the composition-wise solutions can be clearly classified into two groups with very similar compositions, represented by Alloy 1 and Alloy 2 respectively. The composition and ageing condition of two most promising alloys are given in Table 3. Alloy 1 was considered a less attractive solution because its carbon and nickel content are close to the upper limits in the specified design ranges. Moreover, Alloy 1 had a composition similar to that of one of the original alloys yielding the maximum hardness value in the dataset.

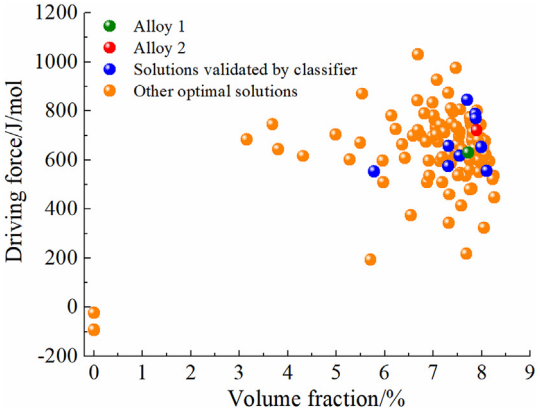

Fig. 3. The spatial distribution of 116 newly designed alloys, with highlight on solutions validated by classifier.

Table 3
Designed alloy composition and ageing conditions and actual alloy composition (based on the recommended composition for alloy 2). Compositions are in weight percentages. Temperature and time are in Celsius and hour, respectively.

	Fe	C	Cr	Ni	Co	Mo	T_{Age}	t_{age}
Alloy 1	Balance	0.090	12.00	6.00	11.50	5.30	500	3.7
Alloy 2	Balance	0.002	13.00	1.50	13.00	5.30	560	4.0
Actual	Balance	0.004	13.20	1.54	12.90	5.49	520–600	0–6

Therefore, Alloy 2 (with a relatively lower total alloy content) was chosen for further experimental validation.

4. Experimental validation

4.1. Experimental procedures

Alloy 2 was smelted and cast into ingots of approximately 5 kg, and the chemical analysis is given in Table 3. The ingot was forged at 1050 °C into a billet with a cross-section of 20 × 20 mm. The square billet was machined into thin slabs with a thickness of 5 mm for heat treatment. To obtain a reasonable comparison with the hardness of samples in the dataset, the process before ageing treatment was executed in a manner consistent with that in the literature from which the dataset was generalized. The alloy was heat treated by austenitization at 1050 °C for 1 h and then refrigerated in liquid nitrogen for 5 h. The ageing treatments were conducted at the design temperature and time. To further explore the formation of the precipitates, the temperature and time of the ageing treatment were expanded to the ranges of 520–600 °C (recommended 560 °C) and 0–6 h (recommended 4.0 h). The Rockwell C hardness, HRC, was measured using an indentation load of 1.5 kN.

The microstructures were investigated by transmission electron microscopy (TEM) and energy dispersive spectroscopy (EDS). TEM investigation was carried out with a JEOL JEM-2200 FS microscope. TEM thin foils of samples taken after the various heat treatments were first mechanically polished to approximately 50 μm thickness. Then, electropolishing was performed with a solution of 10% perchloric acid +90% methanol.

4.2. Hardness

Fig. 4 shows the variation of hardness as a function of ageing temperature and ageing time. The hardness of the quenched Alloy 2 was 34.4 HRC, as shown in Fig. 4a. The hardness of the samples aged at 520 °C increased to 44.1 HRC, as a result of R-phase formation. The peak hardness was obtained at 560 °C with a corresponding maximum value of 52.9 HRC. Regarding the ageing time as shown in Fig. 4b, a sharp increase in hardness was observed for 30 min, indicating that R-phase precipitates rapidly formed at the beginning. The maximal hardness was obtained when the ageing time was 4 h at 560 °C, and the optimal ageing conditions were consistent with Fig. 4a (560 °C at 4 h). The maximum hardness of Alloy 2 was greater than the maximum value in the original dataset (51 HRC, dashed line in Fig. 4). In addition to the successful design of new alloys with a high hardness, the predicted optimal ageing temperature and time were highly consistent with results from the experimental optimization, strongly indicating that the SVM-PM&GA model has a strong ability to accurately and efficiently design the alloy systems and ageing conditions of UHS stainless steel.

The present work demonstrates the methodology as such taking hardness as the target property. However, it can be applied to other target properties as well with appropriate corresponding PM parameters. When multiple properties are required in the design exercise, multiple objective optimization algorithms are required so as to achieve better trade-off among different properties, e.g. to construct Pareto front balancing of different properties.

4.3. Precipitate characterization

The precipitate state of Alloy 2 aged at 560 °C for 4 h was investigated by TEM microscopy combined with EDS analysis. The R-phase precipitate was first identified by Komura et al. [61], and its structure was identified as hexagonal ($a = b = 10.903$ Å, $c = 19.342$ Å) or rhombohedral ($a = 9.005$ Å, $\alpha = 74°$) with a space group of $R\bar{3}$. A high-resolution transmission electron microscopy (HRTEM) image and the corresponding diffraction pattern are shown in Fig. 5a. The precipitates were nearly spheroidal in morphology and mainly formed inside the martensitic laths. Moreover, the crystal structure of the precipitates was identified as R-phase with a hexagonal structure based on the diffraction pattern obtained from the fast Fourier transform (FFT) of the HRTEM image. The chemical compositions of the R-phase obtained from EDS analysis showed that the main alloying elements in the R-phase were Mo, Cr and Co. The Mo and Cr contents were relatively higher than that of Co (Fig. 5b). The morphology and composition results of the R-phase were similar to those of previous studies [62]. In addition, Fig. 5c shows that R-phase precipitates were homogeneously distributed in the lath martensite matrix. The particle size distribution (PSD) of the R-phase is shown in Fig. 5d, which was obtained from approximately 150 R-phase particles. The particle size of most R-phase nanoprecipitates was distributed in the range from 18 nm to 22 nm. The large amount of nanoscale R-phase precipitates with a uniform size distribution should be beneficial to the yield strength, and is consistent with our design philosophy.

5. Discussion

5.1. The effect of PM variables on SVM hardness prediction

To study the influence of PM variables on the generalization ability of the model, the R-phase dataset with or without the additional V_f and D_f data was used to train and test the SVM models, respectively. The modelling process was the same as that in Section

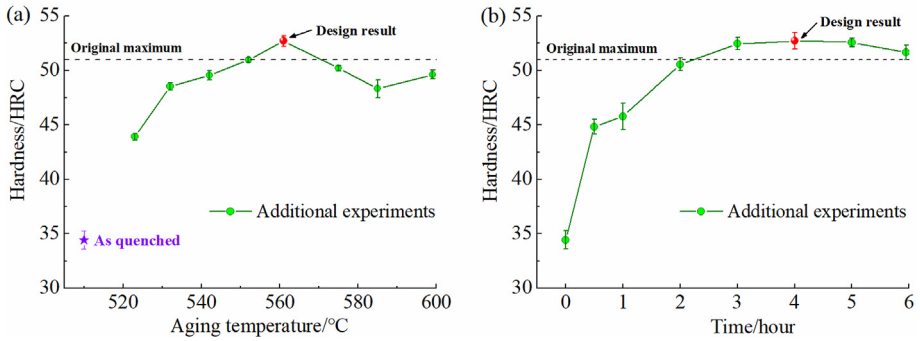

Fig. 4. Experimental hardness of Alloy 2: (a) variation of hardness with ageing temperature at an ageing time of 4 h; (b) variation of hardness with ageing time at an ageing temperature of 560 °C.

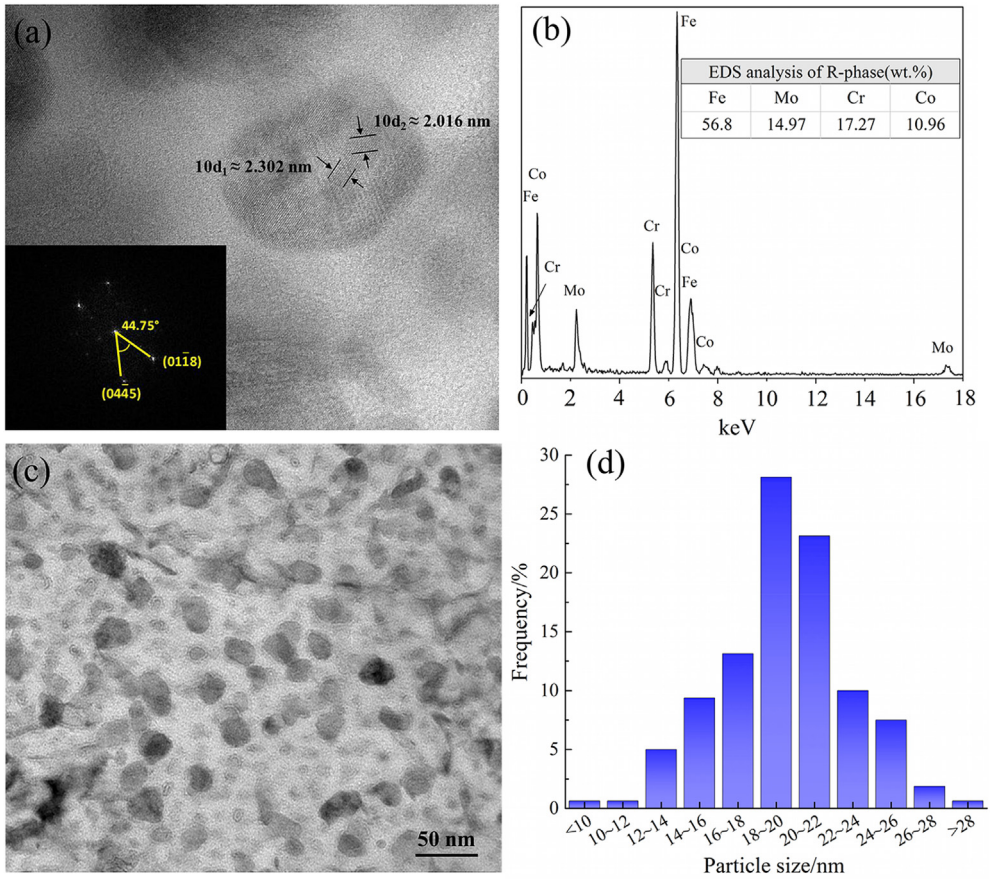

Fig. 5. Precipitate characterization of Alloy 2 after ageing treatment at 560 °C for 4 h: (a) HRTEM image and diffraction pattern; (b) EDS analysis of precipitate; (c) TEM image; (d) PSD result of precipitates.

2.2, and the resulting mean value and standard deviation of the R^2 of the prediction results of 500 partitions of the dataset are shown in Fig. 6a. The introduction of PM variables had no significant effect on the mean value of R^2 and that all four SVM models were at a very high level, approximately 93%. Given the very high level of even without doing so there is only a marginal improvement in R^2 by introducing PM parameters, but it is important to note that the standard deviation was reduced by the addition of PM variables. The standard deviations of the SVM models trained by the dataset without PM variables, with V_f, with D_f and with both PM variables, were 5.9%, 4.7%, 4.6% and 3.9%, respectively. Moreover, overfitting is also an important risk particularly in a small sample problem. The exact number of overfitting SVM models with/without PM parameters, for difference of R^2 value between training set and testing set in the ranges of 10–20%, 20–30% and >30% are plotted respectively as shown in Fig. 6b. It can be clearly observed that the introduction of PM parameters reduces the occurrence of overfitting models, compared to predictions without PM guidelines.

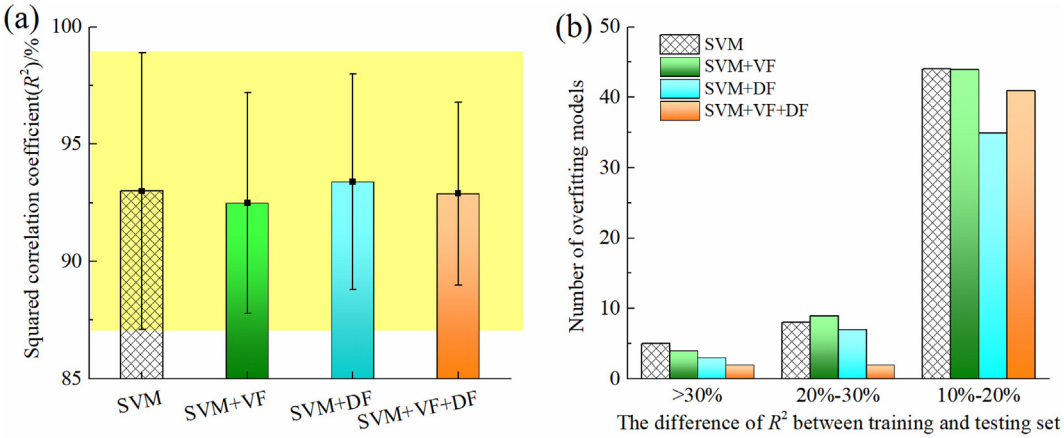

Fig. 6. (a) Squared correlation coefficient (R^2) of the testing sets of the SVM models trained by the dataset with/without PM variables; (b) the number of overfitting ML models with/without PM parameters.

In most previous ML applications to material optimisations, pure ML algorithms not taking into account the underlying material physics were applied to predict material properties, turning materials design into a pure mathematical/statistical process. In the present study, V_f and D_f, as values representing underlying key bridging microstructural features in the 'composition/process-microstructure-mechanical property' relationship, were added to the input vector. The advantage of this approach was that PM parameters are now involved in the modelling process and may play a crucial role in property prediction, which will be further discussed in later sections.

In addition to improving the generalization ability, this new approach also offers a new solution to problems related to a small sample dataset. In general, increasing the data set is a common way to solve small sample problems. However, in materials science, additional information beyond original input, e.g. microstructural characteristics, has to be acquired by standardized experiments; therefore, these methods are time consuming and expensive. Moreover, it is difficult to ensure good data quality due to differences in experimental conditions. In this approach, the dataset's dimension was increased by introducing the corresponding PM variables to each sample using highly reliable thermodynamic calculations that enriched the data information while ensuring data quality. The decrease in the standard deviation and overfitting shown in Fig. 6 was mainly attributed to this effect.

5.2. The effect of PM variables on alloy design

The ultimate goal of the SVM-PM model developed in present work is its application in new alloy design. To elaborate on the effect of introducing PM parameters to alloy design, UHS stainless steel was designed using the SVM&GA model without PM variables with the same process as described in Section 3.1. The difference was that the R^2 for the 216 SVM models was greater than 95% and those models were selected as objective functions in the GA. The ageing temperature, hardness and PM variables of all newly designed alloys, with and without PM parameters' guidance, are compared in Fig. 7. The histogram of the ageing temperature and hardness of all newly designed alloys, with and without PM parameters, are compared in Fig. 7a–b. It can be observed in Fig. 7a that the ageing temperatures of new alloys designed on the basis of SVM-PM are concentrated in the range from 500 to 600 °C, while a much wider variation from 300 °C to 600 °C occurred without the introduction of the PM variables. According to reported experimental data in the literature or thermodynamic calculations the minimum formation temperature of the R-phase in the Fe–Mo–Co–Ni–Cr alloy system is 450 °C [63]. However, approximately 40% of the design results without PM variables had an ageing temperature below 450 °C, which indicated that the R-phase would not effectively act as the strengthening precipitates, and hence, it would not achieve the desirable hardness. In contrast, only 1.9% of the design results with PM variables had an ageing temperature below 450 °C, which clearly reveals the contribution of adding PM variables and enforcing corresponding PM constraints.

The hardness values of the design results with/without PM variables are shown in Fig. 7b. First, designed solutions below the experimental optimal solutions of 51 HRC can be found both without PM variables (31.5%) and with PM variables (27.1%). A detailed comparison yields that the introduction of PM variables is particularly effective in eliminating solutions at the very low side, e.g., below 49 HRC. Second, for the design process with PM variables, most of the designed alloys show hardness values in the range from 51–55 HRC, while the results were more scattered when not using PM variables. On the high end, SVM tends to predict solutions with very high hardness, e.g., 4.6% of the design results were higher than 65 HRC, which seemed attractive; however, the ageing temperature of most of these design results was <450 °C, which was not realistic, as discussed above.

Although the underlying physical data had cast great doubts about the correctness of the proposed solution, the alloy with the maximum hardness (72.5 HRC) predicted by the design process without PM variables was experimentally made as well. The composition of $Alloy_{Max}$ was 0.004C–12.50Cr-2.08Ni-13.06Co-4.87Mo-0.15Ti, and the predicted optimal ageing temperature and time were 300 °C and 3.9 h, respectively. The experimental samples showed a hardness of only 32.2 HRC, which was nearly 40 HRC lower than the predicted value. Microstructure observation with TEM also did not support the presence of R-phases. This result clearly proves that the solutions from a design process without PM variables may be statistically correct but nevertheless may be unreasonable and inconsistent.

To further analyse the mechanism of PM parameters leading to more physically correct solutions, distributions of designed solutions with/without PM parameters are plotted in V_f - D_f space in Fig. 7c. It can be observed that the D_f and V_f of new alloys designed by SVM-PM models are concentrated in the region of high D_f (500–1000 J/mol) and V_f (6.5–8.3%), which would promote the formation of fine dispersion of nano R-phase and hence a high hardness. It is worth noting that approximately 43.0% of the designed results without PM variables' guidance possess negative D_f value, indicating that the R-phase would not actually form, and, most-likely, other undesirable precipitates would form instead. In contrast, only 1.9% of designed results with PM variables show an undesirable D_f value, which clearly demonstrates the role of adding PM variables in improving the rationality of the final alloy composition coming out as the result of the alloy design exercise.

Based on discussion above, it is clear that the PM variables do play an important role in guiding the design process and eliminating the PM impossible solutions.

5.3. The generalization ability for strengthening contributions due to co-existing precipitate families

Traditionally the contributions of different types of coexisting precipitates to the yield strength are calculated separately each for their own physical parameters, and then the (linear) superposition law is applied to estimate the total contribution, which significantly increases the complexity of the prediction process and potentials of error accumulation. Therefore, whether prediction or design using the ML model requires separate calculation of each precipitate species with different dedicated physical parameters is an interesting topic to be addressed.

In this work, three datasets with different precipitate species, i.e., the R-phase, Ni_3Ti intermetallic and Cu clusters, as described in Section 2.1, were used to study the effect of co-existent precipitate species on the generalization ability of SVM. First datasets for a single precipitate family were applied to train the pertinent SVM model for predicting hardness, and the mean R^2 of 100 different partitions of the training and testing sets was used to evaluate generalization ability. The results are shown in Fig. 8a, wherein the R^2 values were 91.1% (±6.2%), 72.6% (±12.9%) and 69.8% (±12%) for the R-phase, Cu cluster and Ni_3Ti datasets, respectively. Furthermore, datasets mixing the R-phase, Cu clusters and Ni_3Ti were also applied to train the SVM model, and the result is shown as 'All' in Fig. 8a. Notably, it is very interesting to note that the mixture of datasets for different strengthening precipitates did not decrease the prediction accuracy, i.e., still around 89.3% (±4.4%), slightly lower than that by using only R-phase dataset. This strongly indicates the strong generalization ability for datasets mixing various precipitates (and the validity of the linear addition rule). In

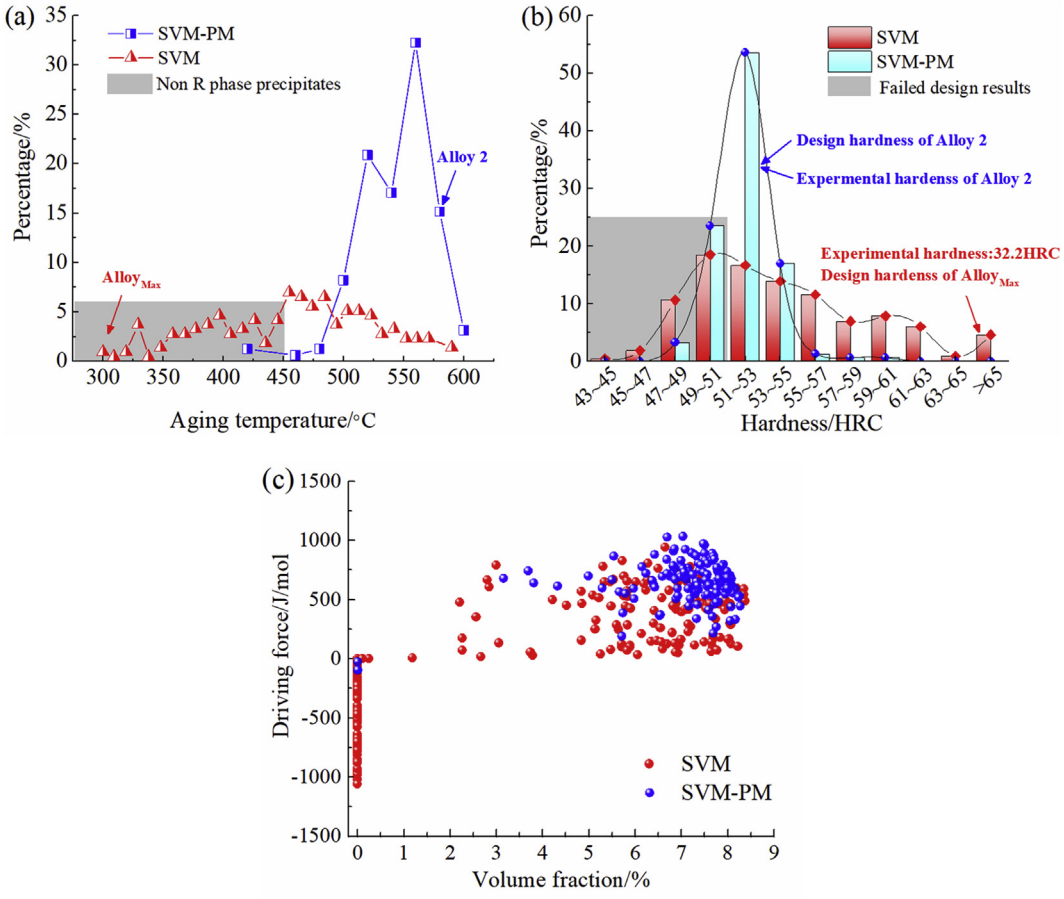

Fig. 7. Comparison of the distribution of all newly designed alloys, with and without PM parameters: (a) ageing temperature; (b) hardness; (c) PM variables.

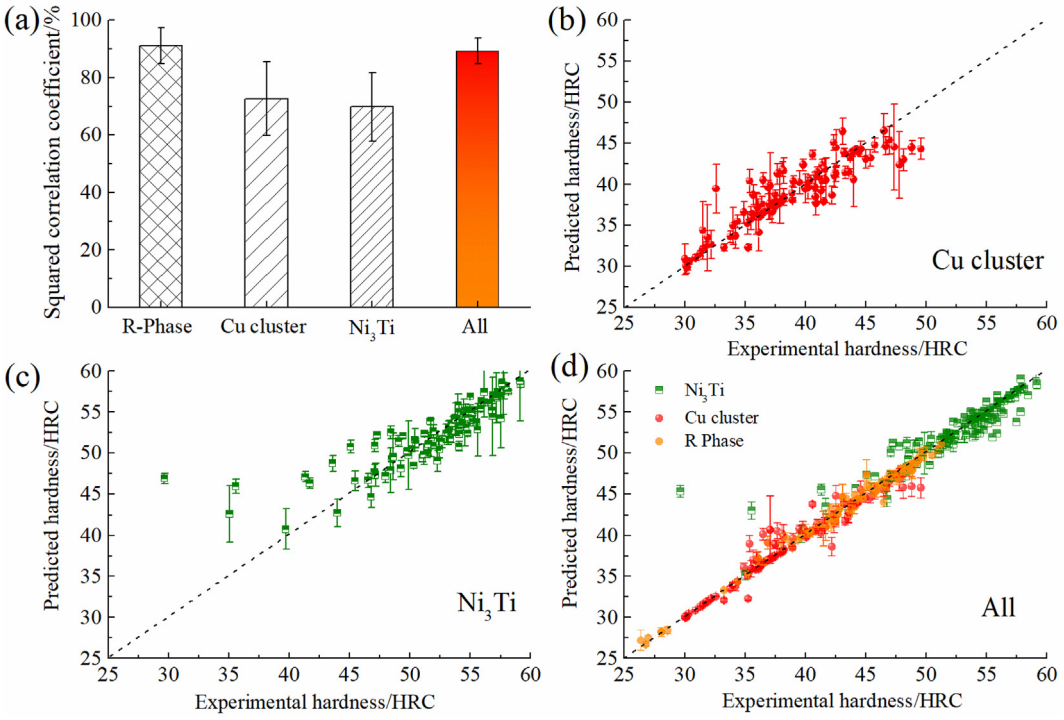

Fig. 8. Prediction results of SVM models trained by datasets with a single precipitate and mixed precipitates (a); experimental value vs. value predicted by the SVM models trained by the Cu dataset (using 124 data) (b), Ni_3Ti (using 116 data) (c) and mixed precipitates (d) datasets (Fig. 1 shows the predictions for the R-precipitates-only steel grades).

addition, the experimental value vs. predicted value plots for the Cu cluster, Ni_3Ti and 'All' datasets are shown in Fig. 8b–d. Compared to Fig. 8b and Fig. 8c, the prediction results for the Cu clusters and Ni_3Ti in Fig. 8d were closer to the diagonal, and the standard deviation of each sample was also smaller. The result by mixing different precipitates is better than those using only low-quality systems (either due to low quantity or low quality), i.e., Cu cluster and Ni_3Ti, which suggests that the good generalization ability actually can be used to increase the prediction reliability of the low-quality system by mixing their datasets with other high-quality systems. This method is completely different from PM models in which a dedicated precipitate system must be calculated separately and parameters of different do not interfere. In summary, the dataset mixing different precipitates did not limit the prediction accuracy but greatly improved the generalization ability, which is advantageous compared to the PM models.

5.4. Generalization sensitivity of various variables

The SVM model establishes the quantitative relationship between inputs and the output in a high-dimensional feature space [64,65], and each feature separately contributes to the model construction in a complex way. For the current dataset, quantitative analysis of the effect of individual input parameters on generalization ability was difficult due to the limited number of samples in the dataset. Instead, a qualitative analysis was carried out by comparing the performance after removing each input dimension from the dataset. The average and standard deviation of R^2 of 500 partitions are shown in Fig. 9. The concentrations of nickel, molybdenum and ageing temperature show the most significant influences on the prediction accuracy, implying their strongest effects on the hardness of UHS stainless steel strengthened by the R-phase. With respect to composition, this phenomenon can be attributed to the great effect of molybdenum and nickel on the precipitation of the R-phase, which is supported by the experimental results [66]. In present dataset, all maraging steels have a strong ability to yield a fully martensitic matrix because Ms temperature of all samples in the dataset is above 350 °C [67]. Besides, carbides are not main strengthening phase, and carbon is also not the main forming element of R-phase. So, carbon variable does not appear to have much effect on hardness. Regarding process parameters, both the ageing temperature and ageing time played key roles in precipitation kinetics. However, only the ageing temperature shows a strong effect, which can be explained by the fact that only two ageing times (3.16 h and 4 h) were involved in the dataset, which made the ageing time nearly invariant and hence it had no effect on SVM performance.

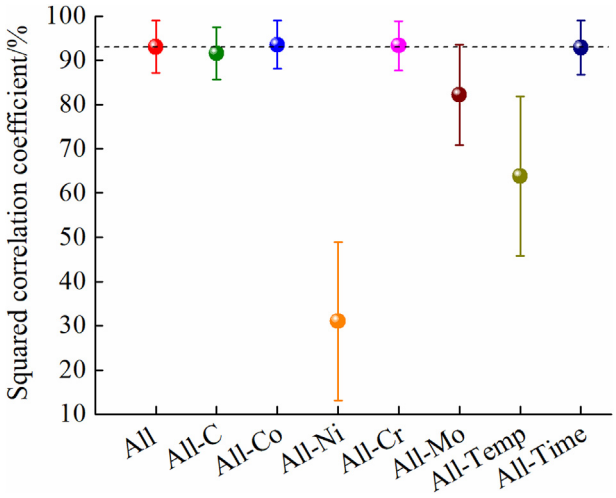

Fig. 9. The variation of the squared correlation coefficient when each feature is removed as input parameter from the dataset.

5.5. The effect of the kernel function on SVM performance

The kernel function, which transfers data into a high-dimensional feature space, determines the type and complexity of SVM models. Therefore, this function is critically important for generalization ability. In this work, four kernel functions, i.e., linear, polynomial, radial basis (i.e., the one used in the above analysis) and sigmoid, were compared using the same training and testing sets to find the most appropriate type. The comparison of predicted and experimental hardness and their associated R^2 values of both the training and testing datasets are shown in Fig. 10. The SVM model with the RBF kernel obtained the best R^2, while the sigmoid kernel performed the worst. The results demonstrate that the selection of the kernel function has a strong influence on the generalization ability, with a difference in R^2 between the RBF kernel and the sigmoid kernel of up to ~80%. Due to its generally good performance, the RBF kernel has also been widely used in the prediction and design of material properties in several previous studies [36,42].

5.6. The effect of the partition method on SVM performance

Lack of data is one of the largest obstacles in the application of ML to the field of materials development. Insufficient data can easily lead to an uneven distribution of samples between the training and testing sets, which will mislead learning process and impede the prediction accuracy. To analyse the effect of the partition method of the training and testing sets on the generalizability in the current system, 100 different random partitions were used to construct SVM models. The optimal C and γ obtained from the GA and the corresponding R^2 values of each partition are shown in Fig. 11. The distribution of R^2 values shows clear fluctuation depending on the partitions but values are mainly confined to the range from 85% to 98%. The corresponding C and γ values also show similar distributions. For several partition configurations, a relatively low R^2 was obtained, which is related to the extreme imbalance of the data distribution between the training and testing sets for such a small dataset. Therefore, for problems with insufficient data, a reliable partition of the training and testing sets is important. However, appropriate evaluation and preselection of data points are difficult. In this situation, the multiple hold-out method that repeats a large number of random partitions is appropriate. Using the multiple hold-out method, the datasets can be randomly and repeatedly divided into training and testing sets, and the average value is taken as an evaluation index, thereby reducing the influence of inappropriate imbalance partition by statistics.

5.7. Comparison between the newly designed alloy and the original alloy

The simplified distance function was used to compare newly designed Alloy 2 and the original alloys in the database. The simplified distance is given by Eq. (4):

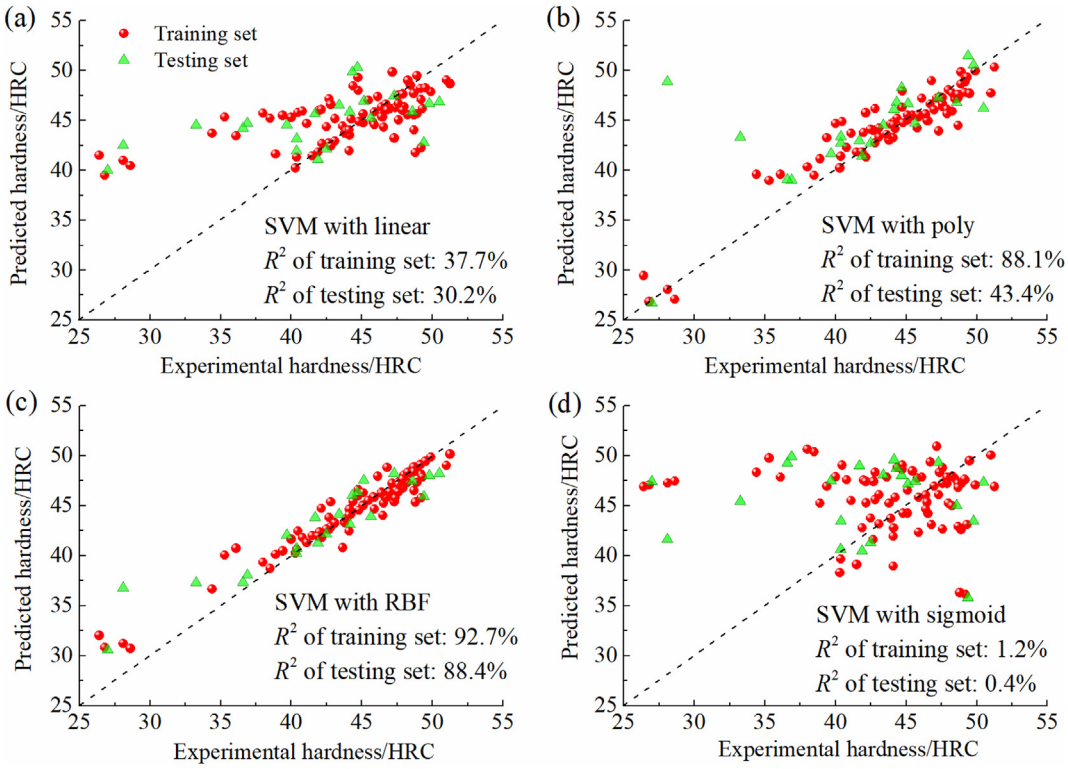

Fig. 10. Experimental vs. predicted hardness with different kernel functions of both the training and testing datasets and their corresponding R^2.

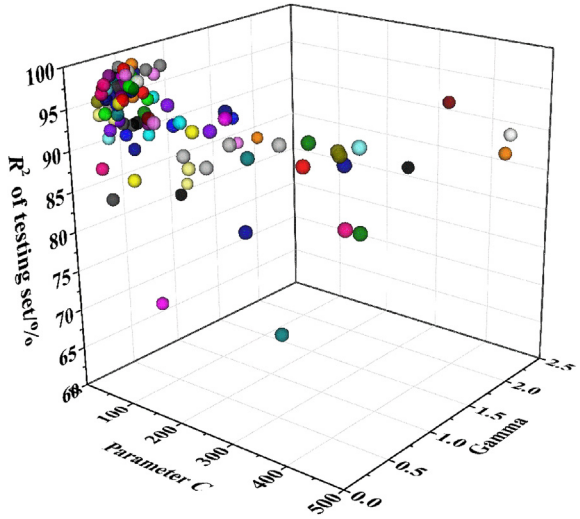

Fig. 11. R^2 of the testing set of 100 SVM models trained by different partitions of the training and testing sets.

$$D = \left(1 - \sqrt{\frac{\sum_{j=1}^{N}\left(Y_{d,j} - Y_{o,j}\right)^2}{N}}\right) \times 100\% \quad (4)$$

where N is the number of elements in the alloy system. $Y_{d,j}$ and $Y_{o,j}$ represent the concentration of the j_{th} element in the design alloy and the original alloy, respectively. Correlation coefficients between Alloy 2 and the twenty original alloys were calculated and shown in Fig. 12a as a radar chart. Alloy 2 did not coincide with any of the twenty original alloys correlation coefficients varied within the range from 65% to 90%, among which original alloy system 15 and original alloy system 6 had the highest and lowest correlations, respectively, with values of 91.1% and 67.4%. A composition comparison between newly designed Alloy 2 and the optimal original alloy is shown in Fig. 12b. Compared with the original optimal alloy, Alloy 2 exhibited a considerable reduction in alloying while achieving a higher hardness. the concentration of C was considerably reduced from 0.09 wt% to 0.002 wt%, and Ni was significantly decreased from 4.6 wt% to 1.5 wt%. Regarding thermodynamics, the V_f of Alloy 2 (7.81%) at 560 °C was larger than that of the optimal sample in the experimental dataset (6.58%), which indicated that more R-phase could form in Alloy 2 during ageing. Moreover, the D_f of Alloy 2 (737 J/mol) was also larger than that of the optimal original sample (638 J/mol), which implied that the R-phase would probably have a higher number density in Alloy 2 because a high nucleation rate is associated with a large transformation D_f. This analysis justifies the potential of the newly designed alloy, not only in terms of properties but also from the perspective of alloying cost.

6. Conclusion

A material design process combining PM-guided ML regression, ML classifier and GA has been proposed in present work. Accordingly, a novel high-strength stainless steel with leaner chemistry was designed and experimentally validated with outperformed hardness.

The implementation of intermediate PM variables, e.g., equilibrium V_f and D_f of precipitates, introduces microstructural considerations in the statistical ML process and hence effectively guides the ML process. For property prediction by ML regression, introducing PM variables effectively improves generalization ability, while for the design process, it eliminates the PM impossible solutions and improves design efficiency.

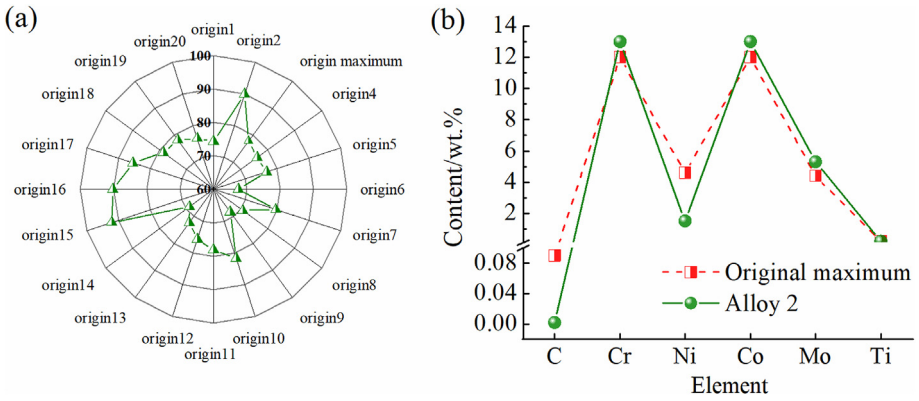

Fig. 12. Correlation between Alloy 2 and the original alloys calculated by the distance function (a); concentration comparison between Alloy 2 and the original optimum (b).

The implementation of PM variables in the dataset increases its dimension and hence improves dataset quality and enriches data information, which is particularly beneficial to address systems with small dataset. Multiple hold-out method is an appropriate method to evaluating model performance in such systems.

The dataset mixing different strengthening precipitates does not limit the prediction accuracy of the ML model but greatly improved the generalization ability, which clearly demonstrates the robustness of the present ML approach.

Relative importance analysis based on the ML model shows that nickel, molybdenum and ageing temperature are closely associated with yield strength, which has been supported by experiments. This result illustrates that the ML model shows promise in the ability to capture the characteristics closely related to targeted outputs.

Compared with previous results, the prototype alloy designed by the present model possesses hardness improvement by ageing at 560 °C for 4 h, which shows exact agreement of designed and experimental optima. Precipitation characterization shows that the target microstructure and high density of nanoscale R-phase precipitates was achieved and homogeneously distributed in the lath martensite matrix.

Acknowledgements

This work was financially supported by the National Natural Science Foundation of China (Grant No. 51574080, Grant No. 51722101). The financial support provided by the National Key R&D Program (Grant No. 2017YFB0703001) is gratefully acknowledged.

Appendix A. Supplementary data

Supplementary data to this article can be found online at https://doi.org/10.1016/j.actamat.2019.08.033.

References

[1] Z. Guo, W. Sha, D. Vaumousse, Microstructural evolution in a PH13-8 stainless steel after ageing, Acta Mater. 51 (2003) 101–116.
[2] H. Leitner, M. Schober, R. Schnitzer, Splitting phenomenon in the precipitation evolution in an Fe-Ni-Al-Ti-Cr stainless steel, Acta Mater. 58 (2010) 1261–1269.
[3] K. Liu, Y.Y. Shan, Z.Y. Yang, J.X. Liang, L. Lu, K. Yang, Effect of aging on microstructure and mechanical property of 1900 MPa grade maraging stainless steel, J. Mater. Sci. Technol. 23 (2007) 312–318.
[4] M. Kapoor, D. Isheim, G. Ghosh, S. Vaynman, M.E. Fine, Y.W. Chung, Aging characteristics and mechanical properties of 1600 MPa body-centered cubic Cu and B2-NiAl precipitation-strengthened ferritic steel, Acta Mater. 73 (2014) 56–74.
[5] J.L. Tian, M. Babar Shahzad, W. Wang, L. Yin, Z.H. Jiang, K. Yang, Role of Co in formation of Ni-Ti clusters in maraging stainless steel, J. Mater. Sci. Technol. 34 (2018) 1671–1675.
[6] H. Leitner, M. Schober, R. Schnitzer, S. Zinner, Strengthening behavior of Fe–Cr–Ni–Al–(Ti) maraging steels, Mater. Sci. Eng. A 528 (2011) 5264–5270.
[7] G.B. Olson, Designing a new material world, Science 288 (2000) 993.
[8] Y. Liu, T.L. Zhao, W.W. Ju, S.Q. Shi, Materials discovery and design using machine learning, J Materiomics 3 (2017) 159–177.
[9] E.I. Galindo-Nava, W.M. Rainforth, P.E.J. Rivera-Diaz-del-Castillo, Predicting microstructure and strength of maraging steels: elemental optimisation, Acta Mater. 117 (2016) 270–285.
[10] C.C. Wang, C. Zhang, Z.G. Yang, J. Su, Y.Q. Weng, Microstructure analysis and yield strength simulation in high Co–Ni secondary hardening steel, Mater. Sci. Eng. A 669 (2016) 312–317.
[11] C. Liu, Q.Q. Shi, W. Yan, C.G. Shen, K. Yang, Y.Y. Shan, M.C. Zhao, Designing a high Si reduced activation ferritic/martensitic steel for nuclear power generation by using Calphad method, J. Mater. Sci. Technol. 35 (2019) 266–274.
[12] J.S. Wang, M.D. Mulholland, G.B. Olson, D.N. Seidman, Prediction of the yield strength of a secondary-hardening steel, Acta Mater. 61 (2013) 4939–4952.
[13] E.I. Galindo-Nava, P.E.J. Rivera-Díaz-del-Castillo, A model for the microstructure behaviour and strength evolution in lath martensite, Acta Mater. 98 (2015) 81–93.
[14] E. Nes, Recovery revisited, Acta Metall. et. Mater. 43 (1995) 2189–2207.
[15] M. Jiang, X.F. Yang, S.Y. Pan, B.W. Krakauer, M.F. Zhu, Correlation between microstructures and yield strength of a high strength enameling steel, J. Mater. Sci. Technol. 28 (2012) 737–744.
[16] R.O. Scattergood, D.J. Bacon, The Orowan mechanism in anisotropic crystals, Philos. Mag. 31 (1975) 179–198.
[17] J. Friedel, Dislocations, Pergamon, New York, 1964.
[18] R.L. Fleischer, Substitutional solution hardening, Acta Metall. 11 (1963) 203–209.
[19] O. Bouaziz, Revisited storage and dynamic recovery of dislocation density evolution law: toward a generalized kocks-mecking model of strain-hardening, Adv. Eng. Mater. 14 (2012) 759–761.
[20] S. Morito, H. Yoshida, T. Maki, X. Huang, Effect of block size on the strength of lath martensite in low carbon steels, Mater. Sci. Eng. A 438 (2006) 237–240.
[21] J.J. Roa, E. Jimenez-Pique, J.M. Tarrago, D.A. Sandoval, A. Mateo, J. Fair, L. Llanes, Hall-Petch strengthening of the constrained metallic binder in WC-Co cemented carbides: experimental assessment by means of massive nanoindentation and statistical analysis, Mater. Sci. Eng. A 676 (2016) 487–491.
[22] C.C. Wang, C. Zhang, Z.G. Yang, J. Su, Y.Q. Weng, Microstructure analysis and yield strength simulation in high Co-Ni secondary hardening steel, Mater. Sci. Eng. A 669 (2016) 312–317.
[23] L.D. Wang, L. Liu, C.X. Ao, X.J. Liu, C.L. Chen, M.K. Kang, Investigation of transformation for ultrahigh strength steel Aermet 100, J. Mater. Sci. Technol. 16 (2000) 491–494.
[24] E.I. Galindo-Nava, P.E.J. Rivera-Diaz-Del-Castillo, Understanding the factors controlling the hardness in martensitic steels, Scr. Mater. 110 (2016) 96–100.
[25] W. Xu, P.E.J. Rivera-Diaz-Del-Castillo, S. van der Zwaag, A combined optimization of alloy composition and aging temperature in designing new UHS precipitation hardenable stainless steels, Comput. Mater. Sci. 45 (2009) 467–473.
[26] Q. Lu, W. Xu, S. van der Zwaag, The design of a compositionally robust martensitic creep-resistant steel with an optimized combination of precipitation hardening and solid-solution strengthening for high-temperature use, Acta Mater. 77 (2014) 310–323.
[27] Q. Lu, S. van der Zwaag, W. Xu, Charting the 'composition-strength' space for novel austenitic, martensitic and ferritic creep resistant steels, J. Mater. Sci. Technol. 33 (2017) 1577–1581.
[28] W. Xu, P.E.J. Rivera-Diaz-Del-Castillo, W. Yan, K. Yang, D. San Martin, L.A.I. Kestens, S. van der Zwaag, A new ultrahigh-strength stainless steel strengthened by various coexisting nanoprecipitates, Acta Mater. 58 (2010)

4067–4075.
[29] Q. Lu, W. Xu, S. van der Zwaag, A strain-based computational design of creep-resistant steels, Acta Mater. 64 (2014) 133–143.
[30] F. Rosenblatt, The perceptron: a probabilistic model for information storage and organization in the brain, Psychol. Rev. 65 (1958) 386–408.
[31] M. Attarian Shandiz, R. Gauvin, Application of machine learning methods for the prediction of crystal system of cathode materials in lithium-ion batteries, Comput. Mater. Sci. 117 (2016) 270–278.
[32] M.A. Yescas, H. Bhadeshia, D.J. MacKay, Estimation of the amount of retained austenite in austempered ductile irons using neural networks, Mater. Sci. Eng. A 311 (2001) 162–173.
[33] E. Bélisle, Z. Huang, S. Le Digabel, A.E. Gheribi, Evaluation of machine learning interpolation techniques for prediction of physical properties, Comput. Mater. Sci. 98 (2015) 170–177.
[34] S.F. Fang, M.P. Wang, W.H. Qi, F. Zheng, Hybrid genetic algorithms and support vector regression in forecasting atmospheric corrosion of metallic materials, Comput. Mater. Sci. 44 (2008) 647–655.
[35] Y.F. Shih, Y.R. Wang, K.L. Lin, C.W. Chen, Improving non-destructive concrete strength tests using support vector machines, Materials 8 (2015) 7169–7178.
[36] Y.T. Sun, H.Y. Bai, M.Z. Li, W.H. Wang, Machine learning approach for prediction and understanding of glass-forming ability, J. Phys. Chem. Lett. 8 (2017) 3434–3439.
[37] Z. Guo, W. Sha, Modelling the correlation between processing parameters and properties of maraging steels using artificial neural network, Comput. Mater. Sci. 29 (2004) 12–28.
[38] Y.F. Wen, C.Z. Cai, X.H. Liu, J.F. Pei, X.J. Zhu, T.T. Xiao, Corrosion rate prediction of 3C steel under different seawater environment by using support vector regression, Corros. Sci. 51 (2009) 349–355.
[39] R.H. Ouyang, S. Curtarolo, E. Ahmetcik, M. Scheffler, L.M. Ghiringhelli, SISSO: a compressed-sensing method for identifying the best low-dimensional descriptor in an immensity of offered candidates, Phys. Rev. Mater. 2 (2018) 1–11.
[40] D. Shin, Y. Yamamoto, M.P. Brady, S. Lee, J.A. Haynes, Modern data analytics approach to predict creep of high-temperature alloys, Acta Mater. 168 (2019) 321–330.
[41] S. Pattanayak, S. Dey, S. Chatterjee, S.G. Chowdhury, S. Datta, Computational intelligence based designing of microalloyed pipeline steel, Comput. Mater. Sci. 104 (2015) 60–68.
[42] D.Z. Xue, P.V. Balachandran, J. Hogden, J. Theiler, D.Q. Xue, T. Lookman, Accelerated search for materials with targeted properties by adaptive design, Nat. Commun. 7 (2016) 1–9.
[43] I. Mohanty, D. Bhattacharjee, S. Datta, Designing cold rolled IF steel sheets with optimized tensile properties using ANN and GA, Comput. Mater. Sci. 50 (2011) 2331–2337.
[44] P. Das, S. Mukherjee, S. Ganguly, B.K. Bhattacharyay, S. Datta, Genetic algorithm based optimization for multi-physical properties of HSLA steel through hybridization of neural network and desirability function, Comput. Mater. Sci. 45 (2009) 104–110.
[45] S. Ganguly, S. Datta, N. Chakraborti, Genetic algorithms in optimization of strength and ductility of low-carbon steels, Mater. Manuf. Process. 22 (2007) 650–658.
[46] T. Lookman, P.V. Balachandran, D.Z. Xue, J. Hogden, J. Theiler, Statistical inference and adaptive design for materials discovery, Curr. Opin. Solid State Mater. Sci. 21 (2017) 121–128.
[47] S.H. Lu, Q.H. Zhou, Y.X. Ouyang, Y.L. Guo, Q. Li, J.L. Wang, Accelerated discovery of stable lead-free hybrid organic-inorganic perovskites via machine learning, Nat. Commun. 9 (2018) 1–8.
[48] W. Garrison, The Effects of Retained Austenite on the Tensile Properties and Toughness of Ultra-high Strength Martensitic Precipitation Hardened Stainless Steels, 1998. United States.
[49] C.N. Hsiao, C.S. Chiou, J.R. Yang, Aging reactions in a 17-4 PH stainless steel, Mater. Chem. Phys. 74 (2002) 134–142.
[50] P. Li, Q.Z. Cai, B.K. Wei, X.Z. Zhang, Effect of aging temperature on erosion-corrosion behavior of 17-4PH stainless steels in dilute sulphuric acid slurry, J. Iron Steel Res. Int. 13 (2006) 73–78.
[51] J. Wang, H. Zou, C. Li, R.L. Zuo, S.Y. Qiu, B.L. Shen, Relationship of microstructure transformation and hardening behavior of type 17-4 PH stainless steel, J. Univ. Sci. Technol. Beijing 13 (2006) 235–239.
[52] U.K. Viswanathan, S. Banerjee, R. Krishnan, Effects of aging on the microstructure of 17-4 PH stainless steel, Mater. Sci. Eng. A 104 (1988) 181–189.
[53] S. Isogawa, H. Yoshida, Y. Hosoi, Y. Tozawa, Improvement of the forgability of 17-4 precipitation hardening stainless steel by ausforming, J. Mater. Process. Technol. 74 (1998) 298–306.
[54] J.H. Wu, C.K. Lin, Influence of high temperature exposure on the mechanical behavior and microstructure of 17-4 PH stainless steel, J. Mater. Sci. 38 (2003) 965–971.
[55] U.K. Viswanathan, G.K. Dey, M.K. Asundi, Precipitation hardening in 350 grade maraging steel, Metall. Trans. A 24 (1993) 2429–2442.
[56] Y. He, K. Yang, W. Sha, Microstructure and mechanical properties of a 2000 MPa grade co-free maraging steel, Metall. Mater. Trans. A 36 (2005) 2273–2287.
[57] F. Zhu, Y.F. Yin, R.G. Faulkner, Microstructural control of maraging steel C300, Mater. Sci. Technol. 27 (2011) 395–405.
[58] A. Jain, K. Nandakumar, A. Ross, Score normalization in multimodal biometric systems, Pattern Recognit. 38 (2005) 2270–2285.
[59] C.J.C. Burges, A tutorial on Support Vector Machines for pattern recognition, Data Min. Knowl. Discov. 2 (1998) 121–167.
[60] A.J. Smola, B. Schölkopf, A tutorial on support vector regression, Stat. Comput. 14 (2004) 199–222.
[61] Y. Komura, W.G. Sly, D.P. Shoemaker, The crystal structure of the R phase, Mo-Co-Cr, Acta Crystallogr. 13 (1960) 575–585.
[62] D.J. Dyson, S.R. Keown, A study of precipitation in a 12 %Cr-Co-Mo steel, Acta Metall. 17 (1969) 1095–1107.
[63] L.V. Tarasenko, V.I. Titov, Intermetallic R-phase in maraging steels of the Fe-Cr-Ni-Co-Mo system, Met. Sci. Heat Treat+ 48 (2006) 374–378.
[64] V. Cherkassky, Y. Ma, Practical selection of SVM parameters and noise estimation for SVM regression, Neural Netw. 17 (2004) 113–126.
[65] V. Cherkassky, Y. Ma, Comparison of model selection for regression, Neural Comput. 15 (2003) 1691–1714.
[66] P. Komolwit, The Effect of Cobalt and Carbon the Microstructure and Mechanical Properties of Martensitic Precipitation Strengthened Stainless Steels, Department of Materials Science and Engineering, Carnegie Mellon University, Pittsburgh, 2009, pp. 26–29.
[67] W. Xu, P.E.J. Rivera-Diaz-del-Castillo, S. van der Zwaag, Designing nano-precipitation strengthened UHS stainless steels combining genetic algorithms and thermodynamics, Comput. Mater. Sci. 44 (2008) 678–689.